sustainability

MDPI

Article

Laboratory Evaluation on the Performance of Porous Asphalt Mixture with Steel Slag for Seasonal Frozen Regions

Hanbing Liu, Bing Zhu, Haibin Wei *, Chao Chai and Yu Chen

College of Transportation, Jilin University, Changchun 130025, China; liuhb@jlu.edu.cn (H.L.); zhubing18@mails.jlu.edu.cn (B.Z.); chaichao18@mails.jlu.edu.cn (C.C.); cheny17@mails.jlu.edu.cn (Y.C.)
* Correspondence: weihb@jlu.edu.cn; Tel.: +86-0431-8509-5446

Received: 31 October 2019; Accepted: 3 December 2019; Published: 5 December 2019

Abstract: Porous asphalt mixtures with steel slag (PAM-SS), as an eco-friendly and low-cost pavement material, are conducive to addressing the issue of urban floods and natural resource shortages. The primary objective of this paper was to explore the feasibility of the application of PAM-SS for seasonal frozen regions, and ascertain the optimal replacement percentage of natural aggregate. Steel slag coarse aggregate (SSCA) was used to replace basalt coarse aggregate (BCA) at four levels (25%, 50%, 75%, 100%) by equal volume. The volume characteristics, mechanical properties, low-temperature cracking resistance, water stability, and freeze-thaw (F-T) durability of the mixture were assessed. The results indicated that the low-temperature cracking resistance of the mixture was significantly enhanced and acoustic emission (AE) energy was uniformly released by the incorporation of steel slag. Furthermore, the porosity, permeability, Marshall stability (MS), and the resistance against water damage and F-T cycles were also significantly improved. Based on the experimental results, the complete replacement of natural aggregate is advisable to obtain an optimal overall performance.

Keywords: porous asphalt mixture; steel slag; low-temperature cracking resistance; water stability; acoustic emission; porosity; permeability

1. Introduction

With the development of urbanization and expansion of urban agglomeration, artificial impermeable pavement has occupied the urban surface at a large scale, blocking the natural infiltration process of rainwater [1]. The resulting "urban diseases", such as urban floods, water resources shortage, and urban heat islands (UHIs), threaten sustainable urban development [2,3]. Porous asphalt mixture (PAM), as a sustainable pavement material for cities, has been developed and applied to parking lots and light traffic pavement due to its potential for alleviating "urban syndrome". Compared with dense-gradation asphalt mixture (DGAM), the high porosity (18–25%) characteristics of PAM make it more competitive in reducing surface stormwater runoff, replenishing groundwater, mitigating the UHI effect, absorbing traffic noise, and improving wet-surface slip resistance [4–6]. Nevertheless, the poor cracking resistance and durability caused by its internal porous structure have become barriers against the wide application of PAM for seasonal frozen regions [4,5]. Therefore, how to improve the low-temperature cracking resistance and freeze-thaw (F-T) durability of PAM for seasonal frozen regions without significantly compromising its permeability has become a research hotspot in this field nowadays.

Under the predicament that limited natural resources cannot keep up with the surging demand of road construction, it is urgent that renewable resources and industrial wastes as an alternative for natural aggregate are found [7,8]. According to the World Steel Association, the world crude steel

output in 2018 reached 1.08 billion tons, of which China accounts for more than half [9,10]. Steel slag is a kind of by-product of the steel industry. However, only 29.5% of the steel slag resources in China have been utilized and others have been dumped on a large scale, occupying land resources and polluting environment [9]. Fortunately, steel slag has superior physical and mechanical properties, such as higher specific gravity, roughness, wear resistance, and crushing resistance, in comparison with natural aggregate [11,12]. If steel slag is feasible in road construction for seasonal frozen regions, it will help to alleviate the issue of natural aggregate shortage and environmental pollution.

The effects of steel slag on the performance of asphalt mixture have been extensively studied in recent years. The chemical composition, microstructure, and surface characteristics of steel slag aggregate were analyzed by X-ray diffraction, mercury intrusion method, and scanning electron microscopy (SEM), respectively, and the results showed that it is a kind of microporous material [13]. Tao et al. [14] conducted dynamic shear rheometer and bending beam rheometer tests to investigate the effect of steel slag filler on the rheological properties of asphalt mortar and found a significant improvement in high-temperature behavior, but a slight drop in low-temperature mechanical performance. Arbani et al. [15] carried out Marshall, dynamic creep, and indirect tensile (IDT) fatigue tests to evaluate the mechanical and dynamic properties of an asphalt mixture containing steel slag. The results reported that the addition of steel slag effectively improved the Marshall stability (MS) and fatigue life and reduced permanent deformation of the asphalt mixture, but the low-temperature cracking resistance was not taken into consideration. Kim et al. [16] studied the impact of steel slag on the expansion characteristics of a hot mix asphalt mixture under humidity and temperature cycles. The results indicated that the strain of the steel slag asphalt mixture was slightly higher than that of the granite asphalt mixture under humidity and temperature cycles. However, the effect of the replacement level with steel slag on strain was not considered. Masoudi et al. [17] found that steel slag enhanced the short-term and long-term aging performances of a warm mix asphalt mixture but slightly raised asphalt consumption. Chen et al. [18] pointed out that steel slag improved the moisture-induced damage resistance. Gao et al. [19] adopted the parallel hot-wire method to evaluate the thermal conductivity of PAM containing steel slag and used software (Inf Rec Analyzer) to quantitatively analyze the heating uniformity. In addition, Phan et al. [20] found that a hot mix asphalt mixture with 30% steel slag had optimal crack-healing performance and ductility. In summary, steel slag, as a novel and promising aggregate, enhances the mechanical properties, fatigue life, aging performances, water damage resistance, and thermal conductivity of asphalt mixture. However, the feasibility of steel slag in seasonal frozen regions needs further study.

Existing researches focus on porous asphalt mixtures with natural aggregate (PAM-NA), but few papers have been published on porous asphalt mixtures with steel slag (PAM-SS). Chen et al. [21] conducted experiments to analyze the lifecycle cost of PAM. The results show that PAM-SS has a lower maintenance cost owing to its higher anti-rutting and anti-clogging performance compared with PAM-NA. Especially in regions where high-quality natural aggregate is scarce, the high quality, low cost, and environmental sustainability of steel slag make it an attractive substitution for natural aggregate. Shen et al. [22] investigated the improvement of steel slag on the noise absorption and interfacial characteristic of PAMs. PAMs with 0%, 25%, 50%, 75%, and 100% steel slag were considered. The results of impedance tube and SEM tests showed that the incorporation of steel slag significantly enhanced the absorption of high frequency noise generated by tire/pavement interaction and the interlocking mechanism between bitumen and aggregate. Moreover, another finding is that the porous structure of PAM reserves enough space for the volume expansion caused by free calcium oxide (f-CaO) and magnesium oxide (MgO), which proves that steel slag is more feasible in PAMs in comparison with DGAM [23].

There are few researches on PAM-SS. In addition, existing studies were mainly concentrated on mechanical behavior, anti-clogging, and noise absorption of PAM-SS, but seldom on low-temperature cracking resistance and F-T durability, especially in seasonal frozen regions. Therefore, low-temperature splitting and acoustic emission (AE) tests were employed to systematically illustrate the low-temperature

cracking mechanism of PAM-SS in this paper. Moreover, the volume characteristics, mechanical properties, moisture susceptibility, and durability were also studied. Finally, the comprehensive feasibility of PAM-SS for seasonal frozen regions was determined. The findings of this research are helpful to understand the effect of steel slag on pavement performance of PAMs, and provide a way to solve the problems of urban flooding and natural aggregate shortages.

2. Materials and Methods

2.1. Raw Materials

The styrene-butadiene-styrene (SBS)-modified bitumen used in this study was obtained from Panjin, Liaoning Province, and its basic properties are shown in Table 1.

Table 1. Properties of SBS-modified bitumen.

Properties	Test Values	Specification
Penetration (25 °C, 0.1 mm)	69.2	60–80
Softening point (°C)	63.5	≥55
Ductility (5 °C, cm)	42.7	≥30
Flash Point (°C)	261	≥230
After TFOT		
Mass loss (%)	0.24	≤±1.0
Penetration ratio (25 °C, %)	67	≥60
Ductility (5 °C, cm)	31	≥20

The coarse aggregates used in this experiment were basalt coarse aggregate (BCA) and steel slag coarse aggregate (SSCA). Both of them were produced in Jilin Province. Their basic properties are listed in Table 2, according to the Standard Test Methods of Aggregate for Highway Engineering (JTG E42-2005) [24]. Figure 1 shows the appearance of 100 g of coarse aggregate. The volume instability of steel slag can be eliminated by placing it in the natural environment for more than 6 months in full contact with rainwater and air [25]. In this study, steel slag was stored for 3 years in the natural environment.

Due to the instability and uncleanness of steel slag fine aggregate, it would weaken the pavement performance of asphalt mixture [26,27]. In addition, the lager specific surface area of steel slag fine aggregate would cause more volume expansion and additional bitumen consumption in comparison with SSCA [28,29]. Considering engineering performance and economy, basalt fine aggregate was used as fine aggregate in this study, and steel slag fine aggregate was not adopted.

Table 2. Properties of coarse aggregates.

Item		BCA	SSCA	Specification
Los Angeles abrasion (%)		17.9	12.7	≤28
Flakiness content (%)		4.8	4.53	≤10
Crushed value (%)		16.8	13.9	≤26
Expansion (%)		0.12	0.44	≤2.0
Apparent density (g/cm^3)	13.2 mm	2.90	3.56	≥2.6
	9.5 mm	2.83	3.55	
	4.75 mm	2.84	3.52	
	2.36 mm	2.69	3.39	
Water absorption (%)	13.2 mm	0.40	1.30	≤2.0
	9.5 mm	0.41	1.47	
	4.75 mm	0.57	1.62	
	2.36 mm	1.01	1.78	

(**a**) (**b**)

Figure 1. Appearance of 100 g of coarse aggregate: (**a**) basalt coarse aggregate (BCA); (**b**) steel slag coarse aggregate (SSCA).

2.2. Mixture Design

Based on the technical specification for permeable asphalt pavement (CJJ/T 190-2012), porous asphalt concrete (PAC)-13 was selected as the experimental gradation (Table 3) [30]. Since SSCA has a higher specific density in comparison with BCA, SSCA was used to replace BCA by an equal volume in order to make the experiment comparable [19,31]. The replacement levels were designed from 0% to 100% (25% increment), labeled as the control group, SSCA-25, SSCA-50, SSCA-75, and SSCA-100, respectively. Based on Cantabro and draindown tests, the optimal bitumen-aggregate ratios (OBRs) of each group were 3.8%, 3.7%, 3.6%, 3.6%, and 3.5%, respectively [32]. Compared with DGAM, PAM reduces bitumen consumption and engineering cost, owing to its less fine aggregate content [33,34]. Another finding is that the OBR decreases slightly with the increase of the replacement level, which is inconsistent with the results obtained by Kavussi et al. [35]. The OBR is the mass ratio of bitumen to aggregate. As is generally known, the rough and porous texture of SSCA increases bitumen consumption, and the high specific gravity of SSCA also increases aggregate mass, when the volume of the mixtures is same [13,15]. When the ratio of the increment of bitumen mass to the increment of aggregate mass is lower than the OBR of the control group, the OBR of the SSCA group would decrease. Conversely, the OBR of SSCA group would increase. The different sources of coarse aggregates make the OBR present different trends.

Table 3. Particle size distributions for PAC-13 at different replacement levels.

Sieve Size (mm)	Upper Limit	Control Group	SSCA-25	SSCA-50	SSCA-75	SSCA-100	Lower Limit
0.075	6	5.0	4.8	4.6	4.4	4.3	2
0.15	8	6.8	6.5	6.3	6.0	5.8	3
0.3	12	7.9	7.6	7.3	7.0	6.8	3
0.6	15	10.5	10.1	9.7	9.3	9.0	4
1.18	18	12.9	12.4	11.9	11.5	11.1	6
2.36	22	16.7	16.0	15.4	14.8	14.3	10
4.75	30	23.4	23.0	22.6	22.2	21.8	12
9.5	80	66.4	66.2	66.0	65.8	65.7	50
13.2	100	94.7	94.7	94.7	94.7	94.7	90
16	100	100	100	100	100	100	100

2.3. Specimen Preparation

The preparation steps of the specimens are listed as follows:

- Step1: Baking. The weighed aggregates and filler were stored in the oven at 180 °C for 6 h, and the SBS-modified bitumen was heated to 180 °C.
- Step2: Mixing. The preheated aggregates were placed in a constant temperature mixing pot and mixed for 90 s. Then, the weighed SBS-modified bitumen was mixed for 90 s. Finally, the preheated filler was also added and mixed for 90 s.
- Step3: Compaction. The Marshall compaction method was adopted, and all specimens were compacted by a standard Marshall hammer, with 50 blows per side.
- Step4: Demolding. All specimens were left to cool at ambient temperature for 12 h before being demolded.

The experimental program is listed in Table 4. According to the specification (JTG E20-2011), there were 18 cylindrical specimens (diameter, 101.6 ± 0.2 mm; height, 63.5 ± 1.3 mm) for each group [36].

Table 4. Experimental program.

Experiments	Number of Specimens Per Group	Experimental Condition
Volume characteristics	3	Three identical specimens were used for Volume characteristics and Marshall tests.
Marshall test	3	
Low-temperature cracking resistance	3	Low-temperature splitting and AE [1] tests were simultaneous.
Water stability and F-T [2] durability	12	4 for IDT [3] test. 4 for IDT test after one F-T cycle. 4 for IDT test after 15 F-T cycles.

[1] Acoustic emission. [2] Freeze-thaw. [3] Indirect tensile.

2.4. Test Methods

2.4.1. Volume Characteristics

The voids of PAM can be divided into connected voids, semi-connected voids, and closed voids [37]. The total porosity is the ratio of the sum volume of connected voids, semi-connected voids, and closed voids of mixture to the total volume of mixture, and the effective porosity is the ratio of the volume of connected voids to the total volume of mixture.

According to Chinese specifications (T 0705-2011 and CJJ/T 190-2012), total porosity and effective porosity were calculated as follows [30,36]:

$$P_T = \left(1 - \frac{\gamma_f}{\gamma_t}\right) \times 100\%, \quad (1)$$

$$P_E = \left(1 - \frac{m_a - m_w}{V\rho_w}\right) \times 100\%, \quad (2)$$

where P_T is the total porosity (%); P_E is the effective porosity (%); γ_f is the bulk specific gravity of the mixture; γ_t is the theoretical maximum specific gravity of the mixture; m_a is the dry mass of the specimen (g); m_w is the mass of the specimen in water (g); V is the measured volume of the specimen (mm^3); and ρ_w is the water density (g/cm^3).

The effective porosity ratio (EPR) is a parameter that can be used to evaluate the degree of voids' continuity distribution and can be expressed by the following equation:

$$EPR = \frac{P_E}{P_T} \times 100\%. \quad (3)$$

According to Chinese specifications (T 0705-2011), voids in mineral aggregates (VMA) and voids filled with asphalt (VFA) were calculated by Equations (4) and (5) [36]:

$$VMA = \left(1 - \gamma_f \times P_s / \gamma_{sb}\right) \times 100, \quad (4)$$

$$VFA = [(VMA - VA)/VMA] \times 100, \quad (5)$$

where γ_f is the bulk specific gravity of the mixture; P_s is the aggregate content percent by weight of the mixture (%); γ_{sb} is the bulk specific gravity of aggregates; and VA is the air voids of the mixture (%).

Permeability is a remarkable characteristic of PAM, which is related to the number, size, and direction of the connected voids [38]. Referring to the technical specification for pervious concrete pavement, the homemade constant head permeable device (shown in Figure 2) was developed based on Darcy's law and used to measure the permeability coefficient [38,39].

The experimental steps were as follows:

- Step1: The plastic film was used to wrap around the side of specimen, and light clay was used to seal the gap between the upper part of the specimen and the lateral wall of the instrument, in order to prevent water from flowing along the side of the specimen.
- Step2: Water was injected to maintain a constant water head.
- Step3: A measuring cylinder was used to collect the water from the lower overflow outlet in 300 s, after water flow was steady.

The permeability coefficient of the specimen was calculated by Equation (6):

$$K = \frac{QL}{AHt}, \quad (6)$$

where K is the permeability coefficient (mm/s), Q is the water volume in the measuring cylinder (mm^3), L is the height of the specimen (mm), A is the upper surface area of the specimen (mm^2), H is the height of water head (mm), and t is the time (s), with t = 300 s.

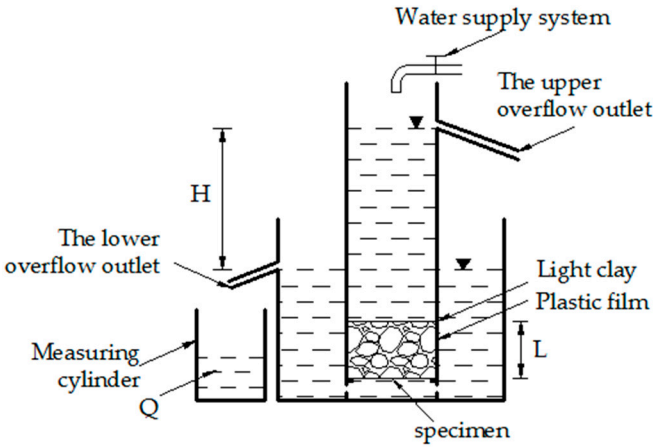

Figure 2. Schematic diagram of the permeability measuring device.

2.4.2. Marshall Test

According to the Chinese specification (CJJ/T 190-2012), Marshall stability (MS) needs to be measured [36]. The Marshall test is commonly used in the mix design of asphalt mixtures and quality inspection for asphalt pavement construction, which was described in detail in our previous study [40].

2.4.3. Low-Temperature Cracking Resistance

The low-temperature splitting test is a simple and common method used for evaluating the low-temperature cracking resistance of asphalt mixtures [36]. The electro-hydraulic servo testing

machine with an environmental chamber was used to carry out the experiment. The test temperature was −10 °C and the loading rate was 1 mm/min. Before the experiment, specimens were stored for 6 h at −10 °C.

According to JTG E20-2011, the coordinate origin was modified by extending the linear segment of the load–displacement curve (shown in Figure 3) [36,41]. The indirect tensile strength (ITS), failure strain, and fracture energy (shadow area in Figure 3) were calculated by the following formulas [41]:

$$ITS = 0.006287F_T/h, \tag{7}$$

$$\varepsilon_T = X_T \times (0.0307 + 0.0936\mu)/(1.35 + 5\mu), \tag{8}$$

$$E = \int_{Y_O}^{Y_T} F_T(y)dy, \tag{9}$$

$$X_T = Y_T \times (0.135 + 0.5\mu)/(1.794 - 0.0314\mu), \tag{10}$$

where ε_T is the failure strain; E is the fracture energy (J); X_T is the horizontal deformation (mm); Y_T is the vertical deformation (mm); μ is the Poisson ratio (μ = 0.25, when the test temperature is −10 °C); h is the height of the specimen (mm); F_T is the peak load (kN); Y_O is the modified initial displacement (mm); and Y_T is the modified critical displacement (mm).

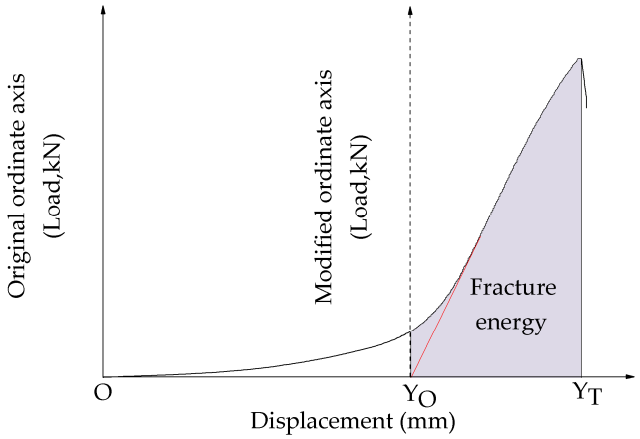

Figure 3. Modification of the load–displacement curve.

Acoustic emission, as a new non-destructive test, is widely used in bridge structural health monitoring but is seldom employed in asphalt mixture [42]. A six-channel AE monitoring was used to acquire signals under low-temperature splitting conditions. AE monitoring consisted of a sensor, preamplifier, acquisition system, and data analysis system. In order to eliminate interference from ambient noise, the threshold value was set to 40 dB. The sensor surface was coated with a sound-transmitting coupling agent (706 silica gel) to ensure full contact with the specimen. An elastic band was used to fix the sensor to the specimen. A detailed description of the low-temperature splitting and AE tests is shown in Figure 4.

The main parameters (shown in Figure 5) of AE were the amplitude, count, rise time, duration, and energy [43]. The AE energy is related to the plastic deformation and crack intensity. The greater the energy, the greater the plastic deformation and crack intensity [44]. AE energy is superior to other parameters in PAM damage identification owing to its high sensitivity to amplitude and duration [43]. In addition, the AE signal at low temperatures is more significant than that at room temperature [45]. Therefore, AE energy was used to describe the fracture characteristics of pervious asphalt mixture under low-temperature splitting conditions, which was defined as follows.

$$\mathrm{E} = \int_0^t V^2(t)dt, \tag{11}$$

where V(*t*) is the recorded voltage, and *t* is the duration time.

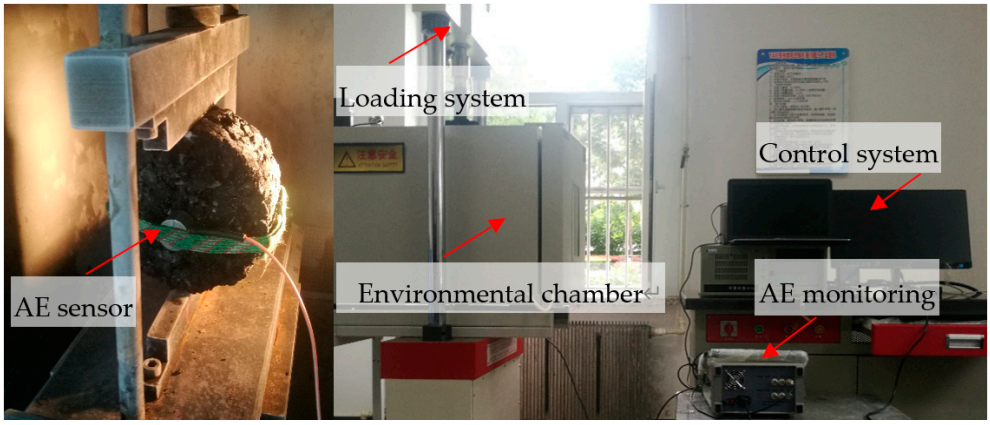

Figure 4. Low-temperature splitting and acoustic emission tests.

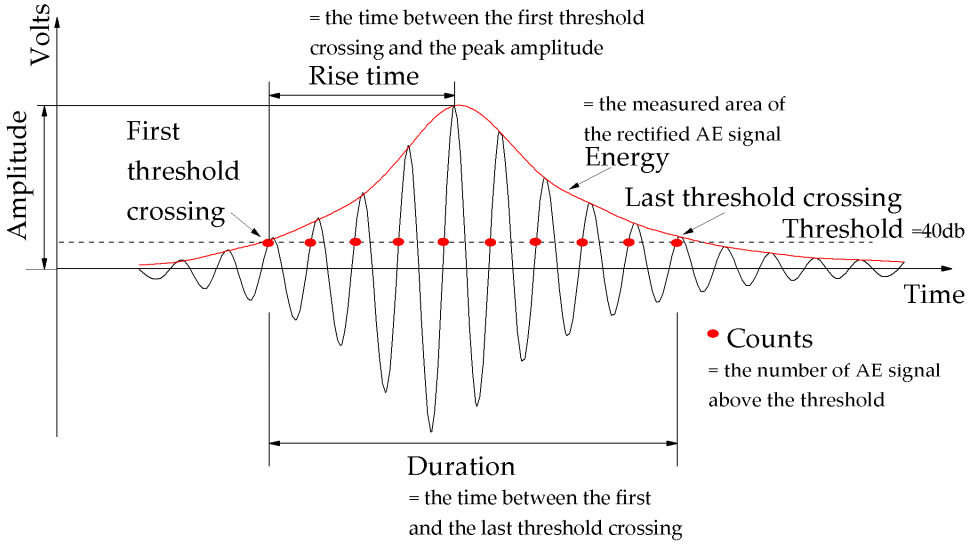

Figure 5. Parameters of acoustic emission.

2.4.4. Water Stability and Freeze-Thaw Durability

According to JTG E20-2011, immersion Marshall and F-T splitting tests are the common methods for evaluating the water stability of asphalt mixtures. Because Jilin Province belongs to a seasonal frozen region, the F-T splitting test can better simulate the actual water damage of PAM in comparison with the immersion Marshall test. Therefore, the F-T splitting test was adopted. For the F-T splitting test, specimens were kept in water at 97.3 to 98.7 kPa (730–740 mmHg) for 15 min, and then immersed into water at atmospheric pressure for 30 min. Subsequently, specimens were frozen at −18 °C in air for 16 h, and then thawed in water at 60 °C for 24 h. The F-T cycles splitting test was the repeated F-T splitting test, which can be seen elsewhere [46]. The difference is that for the F-T cycles splitting test, specimens were thawed at 60 °C for 6 h. A detailed description of the F-T splitting test and F-T cycles splitting test was provided in our previous studies [40,46]. The tensile strength ratio after one F-T cycle (TSR-1) was defined as the ratio between ITS of the specimen subjected to one F-T cycle and ITS of the fresh specimen, and the tensile strength ratio after 15 F-T cycles (TSR-15) as the ratio between ITS of the specimen subjected to 15 F-T cycles and ITS of the fresh specimen. TSR-1 and TSR-15 were adopted to evaluate the water stability and F-T durability of the mixtures, respectively.

3. Results and Discussion

The results of the volume characteristics and Marshall tests are summarized in Table 5, the low-temperature splitting test in Table 6, and the water stability and durability tests in Table 7.

Table 5. Volume characteristics and Marshall test results.

MIX ID	P_T [1] (%)	P_E [2] (%)	EPR [3] (%)	K [4] (mm/s)	MS [5] (kN)
Control	19.89	15.02	75.41	2.85	6.75
SSCA-25	20.78	15.71	75.60	2.97	7.59
SSCA-50	21.6	16.59	76.81	3.12	7.64
SSCA-75	21.8	16.93	77.66	3.23	8.21
SSCA-100	21.81	17.95	77.72	3.25	8.51

[1] Total porosity. [2] Effective porosity. [3] Effective porosity ratio. [4] Permeability coefficient. [5] Marshall stability.

Table 6. Low-temperature splitting test results.

MIX ID	ITS [1] (MPa)	Failure Strain (10^{-6})	Deformation Energy (J)
Control	2.977	2307	12.70
SSCA-25	2.972	2544	14.08
SSCA-50	2.940	2626	14.35
SSCA-75	2.766	3204	16.55
SSCA-100	2.727	3946	18.69

[1] Indirect tensile strength.

Table 7. Water stability and freeze-thaw cycles test results.

MIX ID	ITS (MPa)			TSR-1 [1] (%)	TSR-15 [2] (%)
	Fresh	After One F-T Cycle	After 15 F-T Cycles		
Control	0.633	0.542	0.385	85.63	60.85
SSCA-25	0.635	0.567	0.404	89.34	63.64
SSCA-50	0.659	0.589	0.421	89.37	63.86
SSCA-75	0.706	0.640	0.477	90.65	67.53
SSCA-100	0.749	0.681	0.505	90.85	67.44

[1] Tensile strength ratio after one F-T cycle. [2] Tensile strength ratio after 15 F-T cycles.

3.1. Volume Characteristics

Figure 6a shows the effect of the steel slag replacement percentage on the total porosity and effective porosity. As shown in Figure 6a, with the increase of the steel slag replacement percentage, the trend of total porosity and effective porosity show obviously increasing regularity within 50% replacement, and then begin to level off. Hence, total porosity and effective porosity both reached the maximum (21.81%, 16.95%) and satisfied the standard requirements (18%, 14%) when the replacement level was 100% [30]. Figure 6b shows the relationship between EPR versus the replacement level with SSCC. It can be found that EPR increases with the increment of the steel slag content. The greater EPR value means that more invalid voids were transformed into effective voids and effective voids occupied the majority of the total voids, which could improve the permeability of PAM without significant sacrifice to its mechanical performance. From Figure 6c, VMA increased initially and then decreased slightly with an increasing replacement level with steel slag, but VFA showed an obvious downward trend. It is known that high permeability is a distinguished characteristic for PAM. To ensure high permeability, the permeability coefficient for PAM should meet the criterion of 2.80 mm/s according to Chinese specifications [30]. The permeability coefficient for each group is plotted in Figure 6d. It can be seen that the permeability coefficient also increases with the increase of the substitution rate, which is consistent with the effective porosity. When the substitution rate with SSCA is 100%, the

permeability coefficient reaches the maximum value (3.25 mm/s), which is 14% higher than that of the control group. This is because the permeability coefficient is mainly dominated by the effective porosity, which is consistent with the results obtained by Hamzah [38]. The relationship between the permeability coefficient and effective porosity is presented in Figure 7. Quadratic regression describes the relationship well.

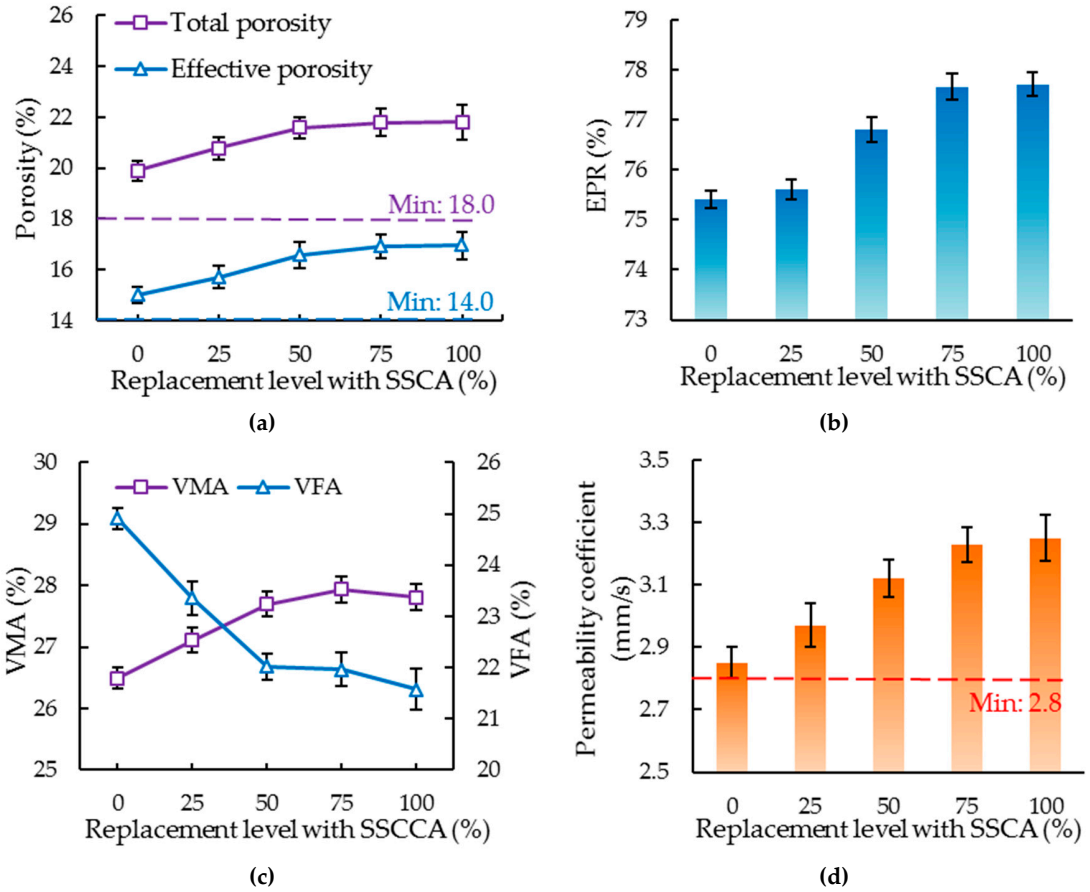

Figure 6. Volume characteristics test results: (**a**) Total porosity and effective porosity; (**b**) Effective porosity ratio (EPR); (**c**) Voids in mineral aggregates (VMA) and voids filled with asphalt (VFA); (**d**) Permeability coefficient.

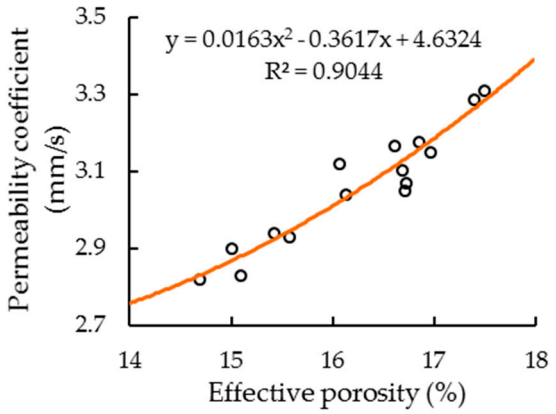

Figure 7. Relationship between the permeability coefficient and effective porosity.

There were several reasons to account for this. Firstly, the multi-angularity of SSCA increased the number and size of voids between the coarse aggregates, which indicated that SSCA was hard to be compacted. This characteristic was disadvantageous to DGM but beneficial to PAM. In addition, the

rough and porous surface of SSCA can convert free bitumen into structural bitumen, dredging the effective voids, increasing the value of EPR, and improving the permeability of PAM. The angularity and surficial texture of the aggregate affect the porosity and permeability of the mixture, which was found in the experiments by Kong et al. [47].

3.2. Marshall Test

The Marshall stability (MS) for all groups is presented in Figure 8. It can be seen that MS increases with the increase of the replacement level with SSCA. Compared with the control group, the MS of the SSCA-25, SSCA-50, SSCA-75, and SSCA-100 group increased by 12.44%, 13.19%, 21.63%, and 26.07%, respectively, which all meet the Chinese standard (≥5.0 kN) [30]. The rough and porous surface of SSCA ensures the cohesive force between aggregate and bitumen. In addition, the high strength of the steel slag aggregate is one of the reasons for the improvement of the MS. Therefore, a 100% replacement level with SSCA is beneficial to the MS.

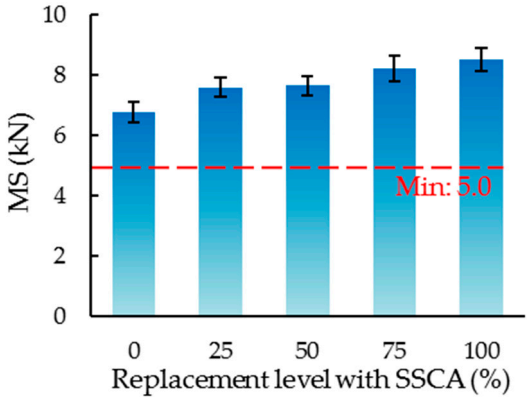

Figure 8. Marshall test result.

3.3. Low-Temperature Cracking Resistance

The ITS and failure strain at low temperatures are shown in Figure 9a. A slight drop in ITS and a significant improvement in failure strain was observed. The higher the failure strength and failure strain, the better the low-temperature cracking resistance. However, the strength and strain of the specimens show inconsistent trends. Conflicting results may be obtained in the evaluation of low-temperature crack resistance when only the failure strain or stress are considered [48]. Therefore, the fracture energy can be used to describe the low-temperature cracking resistance owing to the comprehensive consideration of deformation and strength [49]. Figure 9b shows the variation on fracture energy versus the replacement level. As the replacement level increases, the fracture energy increases significantly. The highest low-temperature cracking resistance and toughness was observed for the specimens containing 100% steel slag and its fracture energy was 1.47 times higher than that of the control group.

The loading–displacement curves for each group are presented in Figure 10. When the substitution level increases from 0% to 100%, the increase in critical displacement (Y_T) was accompanied by a decrease in the slope of the linear section of the load–displacement curve, indicating that the incorporation of SSCA improves the ductility of PAM. Phan et al. found that the metal particles of steel slag have higher ductility than natural aggregates [20].

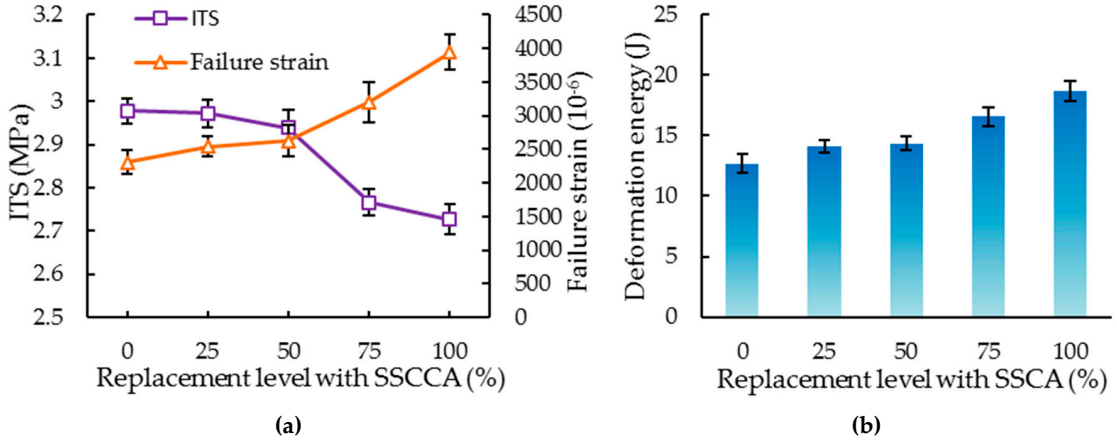

Figure 9. Low-temperature splitting test results: (**a**) Indirect tensile strength (ITS) and failure strain; (**b**) Deformation energy.

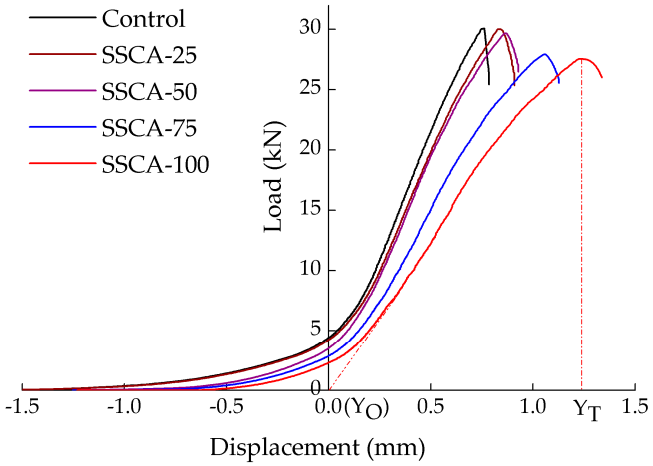

Figure 10. Loading–displacement curves for each group.

Since the AE signals were almost concentrated between Y_O and Y_T, the displacements between Y_O and Y_T were normalized and divided into 10 displacement levels, ranging from 10% to 100% (10% increment). The relative AE energy is the ratio of the AE energy at each displacement level to the total AE energy, and the relative AE energy at each displacement level for all groups is shown in Figure 11. For the control, SSCA-25, and SSCA-50 groups, few relative AE energy was observed under displacement levels between 10% and 20%, indicating the specimen was gradually compacted and the micro-crack intensity was relatively low at these displacement levels. Relative AE energy increased continuously from a displacement level of 20% to 90% due to the stable growth of micro-cracks. When the displacement level exceeded 90%, the relative AE energy increased unexpectedly, which indicated that the macro-cracks extended rapidly until the specimen reached failure. Therefore, the failure process of the control, SSCA-25, and SSCA-50 groups can be divided into three stages. In stage 1, the specimens were compacted. In stage 2, the micro-cracks expanded stably. In stage 3, the rapid extension of macro-cracks led to failure of the specimens. In particular, the relative AE energy of the SSCA-75 and SSCA-100 groups had a local drop at the 70% displacement level and then dramatically surged, which indicated that the crack intensity decreased locally and the specimens showed local resistance, but then the micro-cracks merged into macro-cracks, and the structure could not bear more loads and was almost destroyed. Under the action of the load, the aggregates moved, and the specimens were compacted gradually. At the 70% displacement level, the interlocking structure of SSCA made the specimens show local resistance. However, the formation of macro-cracks broke the interlocking structure and led to the disappearance of local resistance at the 90% displacement level. Whether the local decline of relative AE energy can be used as an early warning of structural

failure needs further study. Based on the above analysis, the failure process of the specimens with 75% and 100% steel slag can be divided into four stages: Compaction, stable propagation of micro-cracks, local resistance, and macro-crack failure, as shown in Figure 11. Besides, the relative AE energy of the steel slag group was higher than that of the control group before the 90% replacement level but lower after the 90% replacement level, which indicated that the release of AE energy of the steel slag group was more uniform. In terms of energy, this uniformity explains the excellent low-temperature cracking resistance of steel slag specimens. This is because the rough and porous texture of steel slag can adsorb more structural bitumen, improving the ductility and AE energy dissipation uniformity of the mixture. In summary, the mixtures containing 100% steel slag present an optimal low-temperature cracking resistance.

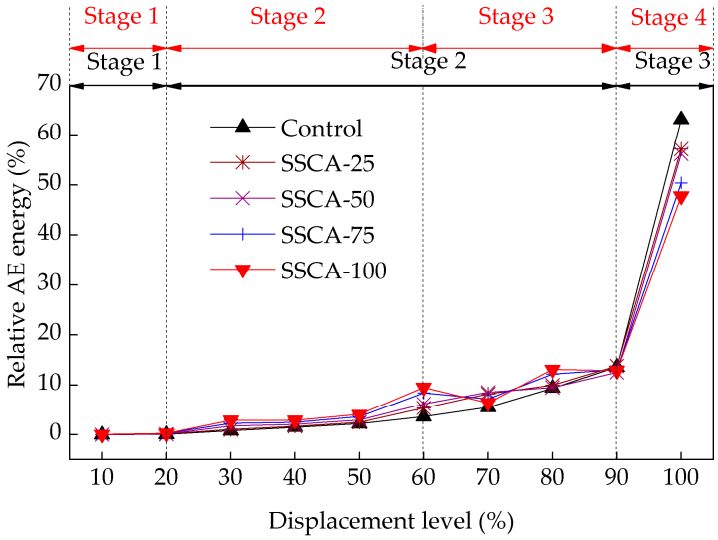

Figure 11. Relationships between relative AE energy and displacement level for each group.

3.4. Water Stability and F-T Durability

The relationship between ITS and the steel slag substitution rate at different F-T levels is shown in Figure 12a. It can be found that ITS decreased with the increase of the F-T cycles, indicating that the durability of mixtures was deteriorated by the F-T cycle. In addition, with the increase of the steel slag substitution rate, ITS shows an upward trend, which is consistent with the Marshall test result. Figure 12b presents the relationship between TSR and the replacement level with SSCA. Under one F-T cycle, the TSR-1 values for all groups were higher than 85%, indicating that the water stability of the sample meets the Chinese specification. TSR-1 and TSR-15 both increased with the increase of the steel slag replacement level, and reached the maximum (90.85%, 67.44%) at the 100% replacement level, which increased by 6.10% and 10.83%, respectively, compared to the control group, indicating that the use of steel slag improves the water stability and F-T durability of the mixtures.

The water stability and F-T durability of the mixtures were related to the adhesion between the bitumen and aggregate, and the adhesiveness depended on intermolecular forces, chemical forces, and mechanical adhesion force. Existing studies have proved that the alkalinity surface of limestone contributes to alleviating moisture deterioration in mixtures [47]. A chemical acid–base interaction also exists between bitumen and steel slag, which is stronger than intermolecular interactions. In addition, the porous characteristics and rough surface texture of the SSCA increase the contact surface with the bitumen, improving the mechanical adhesion [26]. All of that ensures sufficient adhesion between bitumen and SSCA.

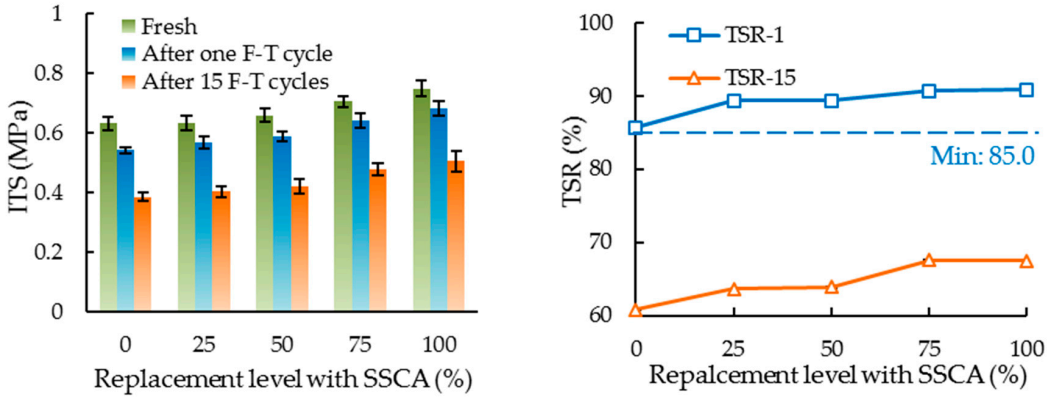

Figure 12. Water stability and freeze-thaw (F-T) durability tests results:(**a**) ITS; (**b**) tensile strength ratio (TSR).

4. Conclusions

In this research, the feasibility of a steel slag porous asphalt mixture for seasonal frozen regions was evaluated. The volume characteristics, Marshall, low-temperature splitting, F-T splitting, and F-T splitting cycles tests were carried out. The influence of SSCA on the pavement performance of the porous asphalt mixture was studied. Based on the test results, the following conclusions can be drawn:

- In contrast to the control group, the steel slag group possesses much higher porosity and permeability. The permeability of mixtures significantly increases with the increase of the substitution rate of steel slag owing to the angularity of steel slag. The permeability coefficients of SSCA-25, SSCA-50, SSCA-75, and SSCA-100 increased by 4.21%, 9.47%, 13.33%, and 14.04%, respectively, compared with the control group.
- The MS of mixtures was increased by the addition of steel slag. The higher the content of steel slag, the greater the MS of the mixture.
- With the increase of the steel slag content, ITS decreases slightly, but the failure strain and fracture energy increase significantly, indicating that steel slag has a positive effect on the low-temperature cracking resistance of mixtures. In particular, the relative AE energy of specimens with 75% and 100% steel slag has a local drop at the 70% displacement level. In addition, the incorporation of steel slag can significantly improve the uniformity of the acoustic emission energy release.
- The mixtures containing 100% steel slag have the largest TSR-1 and TSR-15, which increased by 6.10% and 10.83% compared with the control group. The use of steel slag significantly improves the water stability and F-T durability of the mixtures owing to its alkali and porous characteristics.
- Based on the above conclusions, it is feasible to use a porous asphalt mixture containing 100% steel slag for seasonal frozen regions. PAM containing 100% steel slag has the optimal permeability, strength, low-temperature cracking resistance, and durability, which can accelerate the infiltration of urban rainwater and promote waste recycling. Therefore, it has advantages in alleviating urban flooding and natural resource shortages, and promotes the sustainability of pavement materials.

Author Contributions: Conceptualization, H.L. and B.Z.; methodology, H.L., B.Z., and H.W.; validation, H.L.; formal analysis, H.W.; investigation, B.Z., C.C. and Y.C.; writing—original draft preparation, B.Z.; writing—review & editing, C.C. and Y.C.; project administration, H.W.; funding acquisition, H.L.

Funding: This research was funded by [Science Technology Development Program of Jilin Province] grant number [20180201026SF] and [Transportation Science and Technology Program of Jilin Province] grant number [2018-1-9].

Acknowledgments: The authors would like to appreciate anonymous reviewers for their constructive suggestions and comments to improve the quality of the paper.

Conflicts of Interest: The authors declare no conflict of interest.

References

1. Wang, Q.S.; Ma, Z.; Yuan, X.L.; Wang, J.T.; Mu, Z.Y.; Zuo, J.; Zhang, J.; Hong, J.L.; Wang, S.G. Is cement pavement more sustainable than permeable brick pavement? A case study for Jinan, China. *J. Clean. Prod.* **2019**, *226*, 306–315. [CrossRef]
2. Ding, L.; Ren, X.Y.; Gu, R.Z.; Che, Y. Implementation of the "sponge city" development plan in China: An evaluation of public willingness to pay for the life-cycle maintenance of its facilities. *Cities* **2019**, *93*, 13–30. [CrossRef]
3. Zhang, L.; Sun, X.J.; Xue, H. Identifying critical risks in Sponge City PPP projects using DEMATEL method: A case study of China. *J. Clean. Prod.* **2019**, *226*, 949–958. [CrossRef]
4. Chandrappa, A.K.; Biligiri, K.P. Pervious concrete as a sustainable pavement material—Research findings and future prospects: A state-of-the-art review. *Constr. Build. Mater.* **2016**, *111*, 262–274. [CrossRef]
5. Zhong, R.; Leng, Z.; Poon, C.-S. Research and application of pervious concrete as a sustainable pavement material: A state-of-the-art and state-of-the-practice review. *Constr. Build. Mater.* **2018**, *183*, 544–553. [CrossRef]
6. Xie, N.; Akin, M.; Shi, X. Permeable concrete pavements: A review of environmental benefits and durability. *J. Clean. Prod.* **2019**, *210*, 1605–1621. [CrossRef]
7. Ma, J.M.; Sun, D.Q.; Pang, Q.; Sun, G.; Hu, M.; Lu, T. Potential of recycled concrete aggregate pretreated with waste cooking oil residue for hot mix asphalt. *J. Clean. Prod.* **2019**, *221*, 469–479. [CrossRef]
8. Gómez-Meijide, B.; Pérez, I.; Airey, G.; Thom, N. Stiffness of cold asphalt mixtures with recycled aggregates from construction and demolition waste. *Constr. Build. Mater.* **2015**, *77*, 168–178. [CrossRef]
9. Guo, J.L.; Bao, Y.P.; Wang, M. Steel slag in China: Treatment, recycling, and management. *Waste Manag.* **2018**, *78*, 318–330. [CrossRef]
10. World Steel Association. World Steel in Figures 2019. Available online: https://www.worldsteel.org/en/dam/jcr:96d7a585-e6b2-4d63-b943-4cd9ab621a91/World%2520Steel%2520in%2520Figures%25202019.pdf (accessed on 20 September 2019).
11. Fisher, L.V.; Barron, A.R. The recycling and reuse of steelmaking slags—A review. *Resour. Conserv. Recycl.* **2019**, *146*, 244–255. [CrossRef]
12. Chen, W.; Jin, R.Y.; Xu, Y.D.; Wanatowski, D.; Li, B.; Yan, L.; Pan, Z.; Yang, Y.B. Adopting recycled aggregates as sustainable construction materials: A review of the scientific literature. *Constr. Build. Mater.* **2019**, *218*, 483–496. [CrossRef]
13. Wu, S.; Xue, Y.; Ye, Q.; Chen, Y. Utilization of steel slag as aggregates for stone mastic asphalt (SMA) mixtures. *Build. Environ.* **2007**, *42*, 2580–2585. [CrossRef]
14. Tao, G.Y.; Xiao, Y.; Yang, L.F.; Cui, P.D.; Kong, D.Z.; Xue, Y.J. Characteristics of steel slag filler and its influence on rheological properties of asphalt mortar. *Constr. Build. Mater.* **2019**, *201*, 439–446. [CrossRef]
15. Arabani, M.; Azarhoosh, A.R. The effect of recycled concrete aggregate and steel slag on the dynamic properties of asphalt mixtures. *Constr. Build. Mater.* **2012**, *35*, 1–7. [CrossRef]
16. Kim, K.; Haeng Jo, S.; Kim, N.; Kim, H. Characteristics of hot mix asphalt containing steel slag aggregate according to temperature and void percentage. *Constr. Build. Mater.* **2018**, *188*, 1128–1136. [CrossRef]
17. Masoudi, S.; Abtahi, S.M.; Goli, A. Evaluation of electric arc furnace steel slag coarse aggregate in warm mix asphalt subjected to long-term aging. *Constr. Build. Mater.* **2017**, *135*, 260–266. [CrossRef]
18. Chen, Z.W.; Jiao, Y.Y.; Wu, S.P.; Tu, F.B. Moisture-induced damage resistance of asphalt mixture entirely composed of gneiss and steel slag. *Constr. Build. Mater.* **2018**, *177*, 332–341. [CrossRef]
19. Gao, J.; Sha, A.M.; Wang, Z.J.; Tong, Z.; Liu, Z.Z. Utilization of steel slag as aggregate in asphalt mixtures for microwave deicing. *J. Clean. Prod.* **2017**, *152*, 429–442. [CrossRef]
20. Phan, T.M.; Park, D.-W.; Le, T.H.M. Crack healing performance of hot mix asphalt containing steel slag by microwaves heating. *Constr. Build. Mater.* **2018**, *180*, 503–511. [CrossRef]
21. Chen, J.-S.; Yang, C.H.; Lee, C.-T. Field evaluation of porous asphalt course for life-cycle cost analysis. *Constr. Build. Mater.* **2019**, *221*, 20–26. [CrossRef]
22. Shen, D.-H.; Wu, C.-M.; Du, J.-C. Laboratory investigation of basic oxygen furnace slag for substitution of aggregate in porous asphalt mixture. *Constr. Build. Mater.* **2009**, *23*, 453–461. [CrossRef]
23. Skaf, M.; Ortega-López, V.; Fuente-Alonso, J.A.; Santamaría, A.; Manso, J.M. Ladle furnace slag in asphalt mixes. *Constr. Build. Mater.* **2016**, *122*, 488–495. [CrossRef]

24. Ministry of Transport of the People's Republic of China. *JTG E42-2005. Test. Methods of Aggregate for Highway Engineering*; Ministry of Transport of the People's Republic of China: Beijing, China, 2005. (In Chinese)
25. Ministry of Transport of the People's Republic of China. *JTG F40-2004. Technical Specifications for Construction of Highway Asphalt Pavements*; Ministry of Transport of the People's Republic of China: Beijing, China, 2004. (In Chinese)
26. Xue, Y.J.; Wu, S.P.; Hou, H.B.; Zha, J. Experimental investigation of basic oxygen furnace slag used as aggregate in asphalt mixture. *J. Hazard. Mater.* **2006**, *138*, 261–268. [CrossRef] [PubMed]
27. Xue, Y.J.; Hou, H.B.; Zhu, S.J.; Zha, J. Utilization of municipal solid waste incineration ash in stone mastic asphalt mixture: Pavement performance and environmental impact. *Constr. Build. Mater.* **2009**, *23*, 989–996. [CrossRef]
28. Fakhri, M.; Ahmadi, A. Evaluation of fracture resistance of asphalt mixes involving steel slag and RAP: Susceptibility to aging level and freeze and thaw cycles. *Constr. Build. Mater.* **2017**, *157*, 748–756. [CrossRef]
29. Chen, Z.W.; Wu, S.P.; Wen, J.; Zhao, M.L.; Yi, M.W.; Wan, J.M. Utilization of gneiss coarse aggregate and steel slag fine aggregate in asphalt mixture. *Constr. Build. Mater.* **2015**, *93*, 911–918. [CrossRef]
30. Ministry of Housing and Urban-Rural Development of the People's Republic of China. *CJJ T190-2012. Technical Specification for Permeable Asphalt Pavement*; Ministry of Housing and Urban-Rural Development of the People's Republic of China: Beijing, China, 2012. (In Chinese)
31. Tataranni, P.; Sangiorgi, C. Synthetic Aggregates for the Production of Innovative Low Impact Porous Layers for Urban Pavements. *Infrastructures* **2019**, *4*, 3. [CrossRef]
32. Sangiorgi, C.; Eskandarsefat, S.; Tataranni, P.; Simone, A.; Vignali, V.; Lantieri, C.; Dondi, G. A complete laboratory assessment of crumb rubber porous asphalt. *Constr. Build. Mater.* **2017**, *132*, 500–507. [CrossRef]
33. Wang, W.S.; Cheng, Y.C.; Chen, H.P.; Tan, G.J.; Lv, Z.H.; Bai, Y.S. Study on the Performances of Waste Crumb Rubber Modified Asphalt Mixture with Eco-Friendly Diatomite and Basalt Fiber. *Sustainability* **2019**, *11*, 19. [CrossRef]
34. Yao, Z.H.; Lu, G.L.; Yang, J.; Gong, M.H.; Tang, Z.Y.; Xue, J.Y.; Zhang, X.R. Nanoindentation characterization of aging gradient of mastic in asphalt mixtures. *Constr. Build. Mater.* **2019**, *214*, 187–195. [CrossRef]
35. Kavussi, A.; Qazizadeh, M.J. Fatigue characterization of asphalt mixes containing electric arc furnace (EAF) steel slag subjected to long term aging. *Constr. Build. Mater.* **2014**, *72*, 158–166. [CrossRef]
36. Ministry of Transport of the People's Republic of China. *JTG E20-2011. Standard Test. Methods of Bitumen and Bituminous Mixtures for Highway Engineering*; Ministry of Transport of the People's Republic of China: Beijing, China, 2011. (In Chinese)
37. Liu, H.B.; Luo, G.B.; Wei, H.B.; Yu, H. Strength, Permeability, and Freeze-Thaw Durability of Pervious Concrete with Different Aggregate Sizes, Porosities, and Water-Binder Ratios. *Appl. Sci.* **2018**, *8*, 1217. [CrossRef]
38. Hamzah, M.O.; Hasan, M.R.M.; Ven, M.v.d. Permeability loss in porous asphalt due to binder creep. *Constr. Build. Mater.* **2012**, *30*, 10–15. [CrossRef]
39. Ministry of Housing and Urban-Ural Construction of the People's Republic of China. *CJJ T135-2009. Technical Specification for Pervious Cement Concrete Pavement*; Ministry of Housing and Urban-Ural Construction of the People's Republic of China: Beijing, China, 2009. (In Chinese)
40. Cheng, Y.C.; Chai, C.; Liang, C.Y.; Chen, Y. Mechanical Performance of Warm-Mixed Porous Asphalt Mixture with Steel Slag and Crumb-Rubber-SBS Modified Bitumen for Seasonal Frozen Regions. *Materials* **2019**, *12*, 857. [CrossRef]
41. Cheng, Y.C.; Yu, D.; Tan, G.J.; Zhu, C.F. Low-Temperature Performance and Damage Constitutive Model of Eco-Friendly Basalt Fiber-Diatomite-Modified Asphalt Mixture under Freeze-Thaw Cycles. *Materials* **2018**, *11*, 2148. [CrossRef]
42. Tsangouri, E.; Aggelis, D.G. A review of acoustic emission as indicator of reinforcement effectiveness in concrete and cementitious composites. *Constr. Build. Mater.* **2019**, *224*, 198–205. [CrossRef]
43. Jiao, Y.B.; Fu, L.X.; Shan, W.C.; Liu, S.Q. Damage fracture characterization of pervious asphalt considering temperature effect based on acoustic emission parameters. *Eng. Fract. Mech.* **2019**, *210*, 147–159. [CrossRef]
44. Prem, P.R.; Murthy, A.R. Acoustic emission monitoring of reinforced concrete beams subjected to four-point-bending. *Appl. Acoust.* **2017**, *117*, 28–38. [CrossRef]

45. Jiao, Y.B.; Liu, S.Q.; Fu, L.X.; Shan, W.C. Fracture Monitoring of SBS and Crumb Rubber Modified Porous Asphalt Mixtures under Compression and Splitting Testing Using Acoustic Emission Technique. *J. Mater. Civ. Eng.* **2019**, *31*, 6. [CrossRef]
46. Wang, W.S.; Cheng, Y.C.; Ma, G.R.; Tan, G.J.; Sun, X.; Yang, S.T. Further Investigation on Damage Model of Eco-Friendly Basalt Fiber Modified Asphalt Mixture under Freeze-Thaw Cycles. *Appl. Sci.* **2018**, *9*, 60. [CrossRef]
47. Kong, D.Z.; Xiao, Y.; Wu, S.P.; Tang, N.; Ling, J.T.; Wang, F.S. Comparative evaluation of designing asphalt treated base mixture with composite aggregate types. *Constr. Build. Mater.* **2017**, *156*, 819–827. [CrossRef]
48. Zheng, C.F.; Li, R.M.; Hu, M.J.; Zou, L.L. Determination of low-temperature crack control parameter of binding asphalt materials based on gray correlation analysis. *Constr. Build. Mater.* **2019**, *217*, 226–233. [CrossRef]
49. Park, P.; El-Tawil, S.; Park, S.-Y.; Naaman, A.E. Cracking resistance of fiber reinforced asphalt concrete at −20 °C. *Constr. Build. Mater.* **2015**, *81*, 47–57. [CrossRef]